Layer-by-Layer Conjugated Extension of a Semiconducting Polymer for High-Performance Organic Field-Effect Transistor

Mi Jang, Se Hyun Kim, Han-Koo Lee, Yun-Hi Kim,* and Hoichang Yang**

A donor–acceptor (D–A) semiconducting copolymer, PDPP-TVT-29, comprising a diketopyrrolopyrrole (DPP) derivative with long, linear, space-separated alkyl side-chains and thiophene vinylene thiophene (TVT) for organic field-effect transistors (OFETs) can form highly π-conjugated structures with an edge-on molecular orientation in an as-spun film. In particular, the layer-like conjugated film morphologies can be developed via short-term thermal annealing above 150 °C for 10 min. The strong intermolecular interaction, originating from the fused DPP and D–A interaction, leads to the spontaneous self-assembly of polymer chains within close proximity (with π-overlap distance of 3.55 Å) and forms unexpectedly long-range π-conjugation, which is favorable for both intra- and intermolecular charge transport. Unlike intergranular nanorods in the as-spun film, well-conjugated layers in the 200 °C-annealed film can yield more efficient charge-transport pathways. The granular morphology of the as-spun PDPP-TVT-29 film produces a field-effect mobility (μ_{FET}) of 1.39 $cm^2\ V^{-1}\ s^{-1}$ in an OFET based on a polymer-treated SiO_2 dielectric, while the 27-Å-step layered morphology in the 200 °C-annealed films shows high μ_{FET} values of up to 3.7 $cm^2\ V^{-1}\ s^{-1}$.

1. Introduction

Organic semiconducting polymers have potential advantages for use in large-area and low-cost electronic applications such as displays,[1,2] radio-frequency identification (RFID) tags,[3,4] organic photovoltaics (OPVs),[5,6] and sensors.[7,8] In particular, organic field-effect transistors (OFETs) have achieved and even exceeded the electrical performance of amorphous-silicon-based FETs, with field-effect mobilities (μ_{FET}) above 0.1 $cm^2\ V^{-1}\ s^{-1}$. Significant progress has been made possible owing to solution-processable semiconducting small molecules or oligomers, which can grow into 2D or multilayered, 3D crystals.[9,10] However, it is difficult for substrate-susceptible crystal growth and fragile crystal characteristics to satisfy the deformability required in large-scale flexible electronic applications. Compared to small molecular or oligomeric materials, polymer semiconductors have superior solution processability and mechanical robustness. However, most solution-processed polymer thin films contain nanofibrillar crystal networks separated by less π-conjugated amorphous regions, which is the primary reason for their relatively poor charge-carrier transport properties.[11]

The application of diketopyrrolopyrrole (DPP)-based polymers in organic electronics has been gaining attention owing to the polymers' excellent electrical performance in OFETs and OPVs. Compared to other semiconducting polymers, the synthesis of DPP is relatively simple and inexpensive.[12] DPP is a versatile acceptor (A) building block that is applicable for a wide range of structural modifications by attaching alkyl chains to the lactam N-atoms to facilitate easy solution processability and by connecting various donor (D) blocks at the 2- and 5-positions of the DPP.[13,14] In addition, the solid-state packing and optical properties of π-conjugated polymers are dependent on the nature of both the attaching alkyl chains in the DPP core and the next-neighbor conjugated blocks.[15] Many DPP-based copolymers have competed with high-mobility semiconductors in the selection of materials for commercially feasible organic electronics. Recently, we reported that after thermal annealing, a film of a DPP-based copolymer, poly[2,5-bis(7-decylnonadecyl)pyrrolo[3,4-*c*]pyrrole-1,4(2*H*,5*H*)-dione-(*E*)-1,2-di(2,2′-bithiophen-5-yl)ethene] (PDPPDBTE-29 or PDPP-TVT-29), exhibited an exceptionally high μ_{FET} of >3.0 $cm^2\ V^{-1}\ s^{-1}$.[16] It was expected that the introduction of alkyl chains with a long, linear space group in PDPP-TVT-29 could improve the interdigitation of the polymer chains to form a π-conjugated crystal structure under various film-processing conditions.[17,18] Although this result must be a

M. Jang, Prof. H. Yang
Department of Applied Organic Materials Engineering
Inha University
Incheon 402-751, South Korea
E-mail: hcyang@inha.ac.kr
Prof. S. H. Kim
Department of Nano
Medical and Polymer Materials
Yeungnam University
Gyeongsan 712-749, South Korea
Dr. H.-K. Lee
Pohang Accelerator Laboratory
Pohang 790-784, South Korea
E-mail: hangulee@postech.ac.kr
Prof. Y.-H. Kim
Department of Chemistry
Gyeongsang National University and Research Institute of Nature Science (RINS)
Jinju 660-701, South Korea
E-mail: ykim@gnu.ac.kr

DOI: 10.1002/adfm.201403497

remarkable advance in semiconducting-polymer-based organic electronics, the crystalline structures in the solid state of PDPP-TVT-29 films have not been studied in detail. Therefore, it is necessary to optimize the crystal structure of DPP-based copolymers to yield good π–π stacks along the direction of charge transport.

In the present study, we systematically investigated the crystalline morphologies and orientations of the DPP-based copolymers in solution-cast films in order to obtain the large, π-conjugated, overlapping morphology of polymer semiconductors. Morphological and X-ray analyses clearly demonstrated that a solution-cast PDPP-TVT-29 film can become a highly ordered and multilayered structure with an edge-on orientation through thermal annealing. On a polystyrene (PS)-grafted SiO_2 dielectric, the strong intermolecular interaction such as π–π overlap between DPP moieties[19] and intramolecular D–A interaction led to the spontaneous self-assembly of the DPP-based copolymer chains with a close π-overlap distance of 3.55 Å and unexpectedly large layer-like structures, which are favorable for intermolecular charge transport. As a result, the as-spun PDPP-TVT-29 film that displayed granular layer morphology had a field-effect mobility (μ_{FET}) that remained above 1.3 $cm^2\ V^{-1}\ s^{-1}$ in the corresponding OFET, whereas the layer-by-layer morphology developed via thermal annealing allowed μ_{FET} to be improved to 3.7 $cm^2\ V^{-1}\ s^{-1}$.

2. Results and Discussion

The PDPP-TVT-29-based organic field-effect transistors with a bottom-gate and top-contact structure were fabricated on 300 nm thick SiO_2 dielectrics, each of which was modified with a PS-grafted layer (gPS) (**Figure 1**). Dimethylchlorosilane-terminated polystyrene was used as the dielectric surface modifier. The semiconductor channel layer was deposited by spin-casting

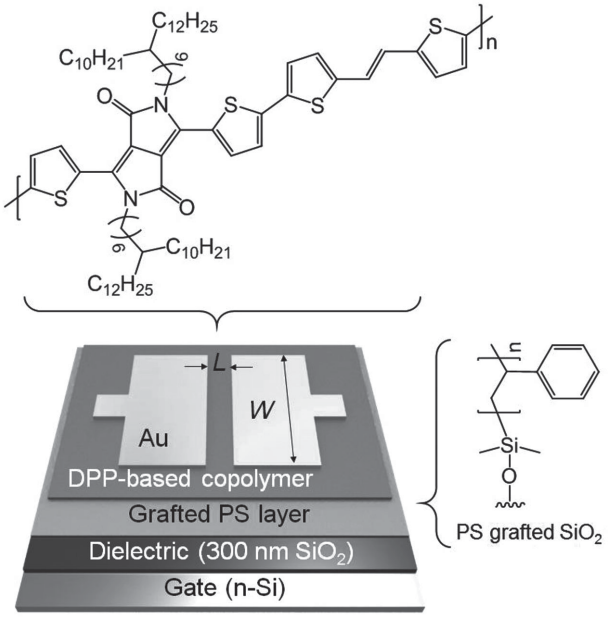

Figure 1. Schematic diagram of a bottom-gate, top-contact organic field-effect transistor fabricated in this study.

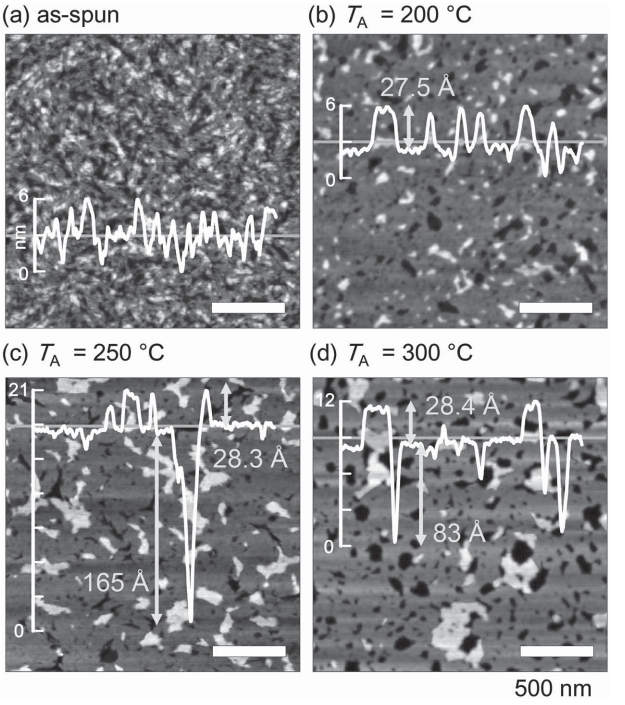

Figure 2. AFM images showing the topographies of spun-cast PDPP-TVT-29 films on the gPS-SiO_2 dielectric substrates a) before and b–d) after thermal annealing at different values of T_A for 10 min: a) as-spun; b) 200 °C; c) 250 °C; d) 300 °C.

a solution of PDPP-TVT-29 in chloroform (2 mg mL^{-1}). Some cast films were then thermally annealed at various annealing temperatures (T_A) for 10 min, based on differential scanning calorimetry analysis for a PDPP-TVT-29 powder (see Figure S1, Supporting Information).

Figure 2 shows typical atomic force microscopy (AFM) images that show the topographies of PDPP-TVT-29 films (thickness: 15–20 nm) on the gPS-SiO_2 dielectric substrates before and after annealing at various T_A. The as-spun film consisted of intergranular nanocrystals with a mesoscopic structure between the rods and layers (Figure 2a). In contrast, short-term thermal annealing at different values of T_A could control their crystalline morphologies dramatically. As shown in Figure 2b–d, the less-ordered nanocrystals (in the as-spun film) evolved into continuous layers, but deeper pinholes, which acted as physical charge-trap sites, were observed with increasing T_A (Figure S2, Supporting Information). Additionally, the layer-step height (L_H) had values between 27.5 and 28.4 Å regardless of the value of T_A (summarized in **Table 1**).

Two-dimensional grazing-incidence X-ray diffraction (2D GIXD) patterns of these PDPP-TVT-29 films on the gPS-SiO_2 dielectric substrates showed intense X-ray reflections along the Q_z (out-of-plane) and Q_{xy} (in-plane) axes (**Figure 3**). It should be noted that the beam center and (100) peak position of the patterns were blocked with an Al beam stopper to avoid detector saturation owing to their strong intensities, which means that the actual (100) peak intensities for all the films were higher than indicated. All of the PDPP-TVT-29 films maintained an "edge-on" conformation with a π-conjugated direction parallel to the gPS-SiO_2 dielectric surfaces. Combining the 1D

Table 1. Structural characteristics of as-spun and annealed PDPP-TVT-29 films.

Film	Annealing condition [°C]	L_H [Å][a)]	$d_{(100)}$ [Å][b)]	$d_{(010)}$ [Å]	$R^{c)}$	α [°][c)]
As-spun	–	–	28.0	3.54	0.217 ± 0.2	60.4 ± 0.26
	200	27.5	27.6	3.55	0.322 ± 0.2	63.1 ± 0.36
T_A-annealed	250	28.3	27.5	3.56	0.228 ± 0.2	60.7 ± 0.28
	300	28.4	28.0	3.56	0.142 ± 0.2	58.5 ± 0.16

[a–c)]Calculated from AFM, GIXD, and NEXAFS analyses, respectively.

out-of-plane X-ray reflections of (h00) planes with the AFM morphologies (Figure 2 and Figure S3, Supporting Information), it was determined that PDPP-TVT-29 could form a long-range π-conjugated film structure with a (100) domain spacing, $d_{(100)}$, that ranged from 27.5 to 28.0 Å (Table 1).

Compared to the as-spun film, the annealed PDPP-TVT-29 films exhibited sharper and more oriented X-ray reflections of (010) crystal planes along the out-of-plane direction at Q_{xy} = 1.795 Å^{-1}. In particular, the domain spacing between the (010) crystal planes, $d_{(010)}$, (referred to as the intermolecular π-conjugated distance) was ≈3.55 Å, which is much shorter than those of other semiconducting polymers ($d_{(010)}$ ≈ 3.85 Å for poly(3-hexylthiophene), or P3HT,[20] and ≈3.72 Å for poly(2,5-bis(3-alkylthiophen-2-yl)thieno[3,2-b]thiophenes), or pBTTT.[21] In addition, it was very close to those of oligomeric semiconductors with highly crystalline structures, e.g., triisopropylsilylethynyl pentacene (TIPS-PEN; $d_{(010)}$ ≈ 3.50 Å) and triethylsilylethynyl anthradithiophene (TES-ADT; $d_{(010)}$ ≈ 3.45 Å).[9–11,21,22] McCulloch et al. reported that among the semiconducting polymers, pBTTT with $d_{(010)}$ of about 3.72 Å showed the highest μ_{FET} of up to 0.7 cm^2 V^{-1} s^{-1} in OFETs. This was attained by developing 2D micrometer-sized crystals with fewer grain boundaries (GBs) instead of 1D nanogranular fibrils.[21] Therefore, it can be expected that for a layered π-conjugated film of PDPP-TVT-29, with better lateral π-conjugated overlap along the source–drain (S–D) electrodes in an OFET, high electrical properties would be obtained, in addition to intrinsically high charge transport along the polymer backbone with a low band-gap of 1.28 eV.[21] Nevertheless, the thermally annealed PDPP-TVT-29 films, with layered morphologies as determined by AFM, could not provide clear evidence related to the long-range in-plane π–π stacking in 2D GIXD patterns, although the out-of-plane X-ray profiles showed high crystallinity and crystal orientation in the sample that was annealed at 200 °C (Figure S4, Supporting Information). This result is quite similar to those recently reported by other research groups.[23,24]

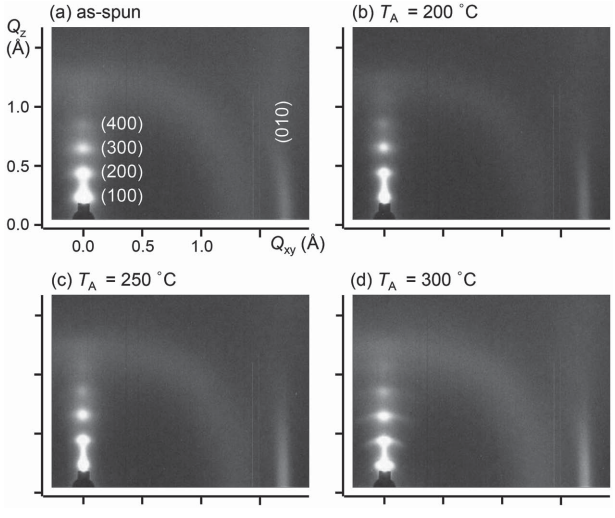

Figure 3. 2D GIXD patterns of spun-cast PDPP-TVT-29 films on gPS-SiO_2 dielectric substrates a) before and b–d) after thermal annealing at different values of T_A for 10 min: a) as-spun; b) 200 °C; c) 250 °C; d) 300 °C.

To further investigate the in-plane π-conjugated overlap of PDPP-TVT-29 polymers, near-edge X-ray absorption of fine structure (NEXAFS) spectroscopy was performed on the as-spun and thermally annealed PDPP-TVT-29 films. NEXAFS spectroscopy is an element-specific and bond-sensitive technique, which probes an ≈6 nm thick layer near the surface in its partial-electron-yield (PEY) detection mode.[25] In particular, NEXAFS can measure the average orientation of the π-conjugated planes in organic semiconductors by collecting carbon K-edge spectra obtained from various angles of incidence of the synchrotron photon beam from the surface plane.[26,27] Furthermore, detailed structural information, such as the tilting angle of the conjugated planes, can be derived from the spectra.[26,27] **Figure 4** shows representative NEXAFS spectra acquired from the PDPP-TVT-29 films. The features in the NEXAFS spectra are assigned to the π^* (C=C) orbital at 285.4 eV, the σ^* (C–S) and π^* (C=O) orbitals mixed with Rydberg orbitals around 287–291 eV, and several σ^* orbitals in the energy range of 292–307 eV. To determine the tilt angle (α) between the C=C double bond in the conjugated planes and the SiO_2 (substrate) surface, a fourfold symmetry of the substrate was used with the photon beam, which had a beam size of ≈0.1 × 0.3 mm^2. The peak intensities of the π^* (C=C) orbital in the NEXAFS spectra were then fitted by the following equation

$$I_\nu \propto \left[\frac{P}{3}\{1+\frac{1}{2}(3\cos^2\theta-1)(3\cos^2\alpha-1)\}+\frac{(1-P)}{2}\sin^2\alpha\right] \quad (1)$$

where θ is the polarization angle of the incident synchrotron light with respect to the normal to the surface, and P = 1 is used for the degree of polarization.[25]

In addition, the angular dependence of the 1s → π^* intensities is usually expressed by a dichroic ratio, $R=\frac{I(90^\circ)-I(0^\circ)}{I(90^\circ)+I(0^\circ)}$, which is the difference between the intensities at θ = 90° and 0°, divided by their sum. The calculated R and α values are summarized in Table 1. The value of R varies from +1 (for horizontal π^* orbital and α = 90°), to 0 (for random orientation, known as magic angle α = 54.7°) and −1 (for a vertical π^* orbital and α = 0°): a more positive R signifies a larger average tilting angle of the transition dipole away from the substrate.[25] Additionally, the side-chain orientation is reflected in the 1s → σ^* intensities, but it is complicated to quantify because of its random coil-like structure and backbone contributions.

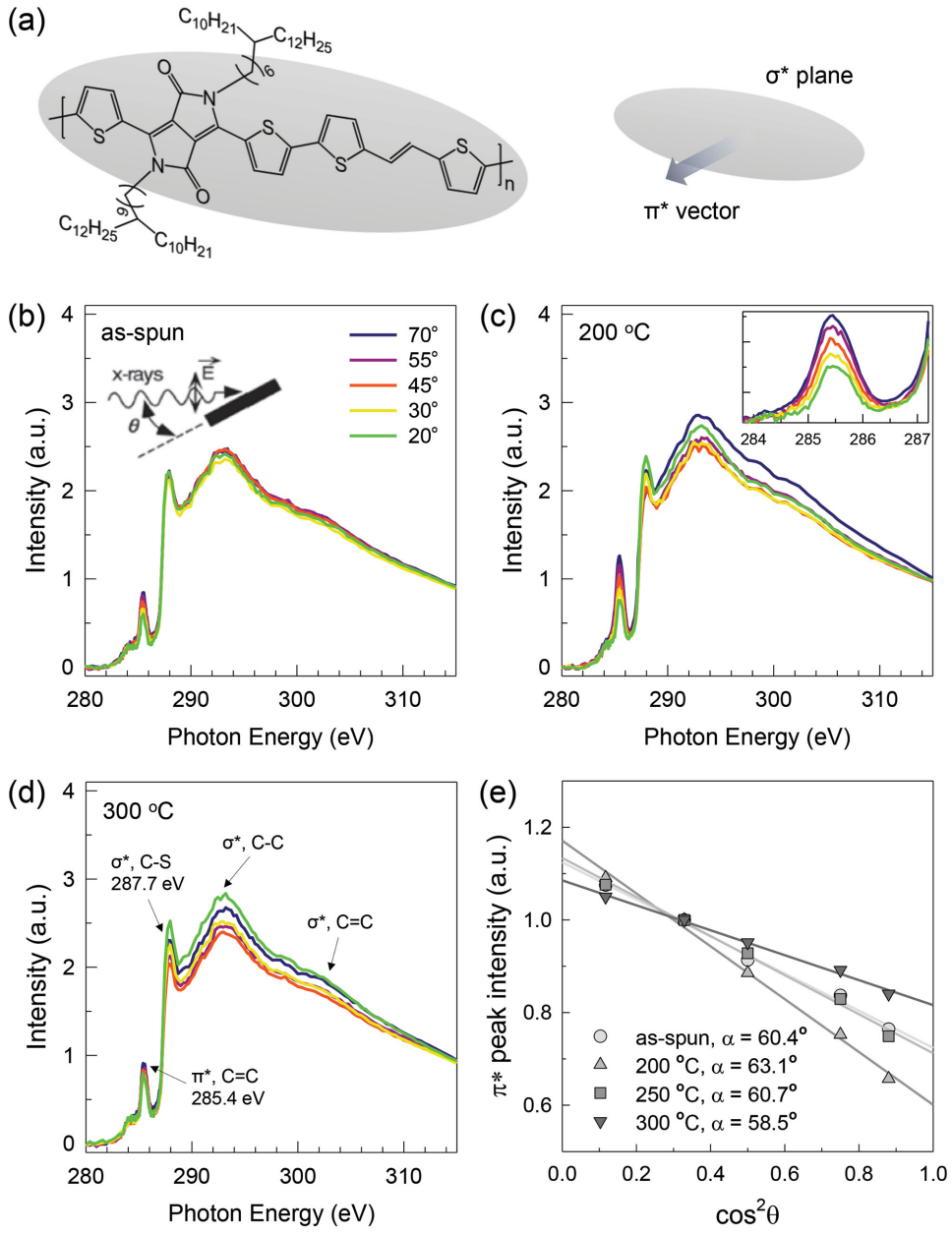

Figure 4. a) Antibonding orbital directions of PDPP-TVT-29. b–d) Angle-dependent carbon *K*-edge NEXAFS spectra acquired from the top interfaces of polymer films: b) as-spun; c) annealed at 200 °C; d) annealed at 300 °C. (The partial-electron-yield mode had a standard uncertainty of ±2%; the photon energy had a standard uncertainty of ±0.1 eV.) e) Intensities of π^* transitions versus incidence angle. The solid lines represent the fitted curves.

It was found that the peak intensity of the π^* resonance increased with an increase in θ, as shown in Figures 4b–d, thus revealing an edge-on orientation of conjugated planes. From the best fit (solid line in Figure 4d), α values for the as-spun film and the films that were annealed at 200, 250, and 300 °C were 60.4° ± 0.26° (R = 0.217), 63.1° ± 0.36° (R = 0.322), 60.7° ± 0.28° (R = 0.228), and 58.5° ± 0.16° (R = 0.142), respectively. These values are consistent with the molecular orientations inferred from the 2D GIXD patterns, indicating a preferentially edge-on orientation of the conjugated plane of PDPP-TVT-29 films.

On the basis of these morphological and structural results, it is expected that the T_A-mediated crystal structures can yield highly lateral π-conjugated layers of PDPP-TVT-29 films, as well as good charge-transport properties of the corresponding OFETs (**Figure 5**).

Top-contact-electrode OFETs (L = 100 µm and W = 1500 µm, Figure 1) were fabricated to determine the charge-transport characteristics in the T_A-mediated crystal structures of PDPP-TVT-29 on the gPS-SiO_2 dielectrics with C_i value of 10 nF cm^{-2}. **Figure 6**a–c shows typical drain current–gate voltage (I_D–V_G) transfer curves of the OFETs with T_A-mediated PDPP-TVT-29 films, operated at the saturation regime (drain voltage V_D = −30 V). **Table 2** lists the electrical properties of the OFETs. All the devices showed typical p-type transistor behavior, with

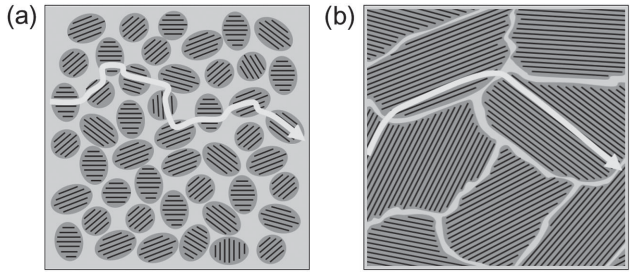

Figure 5. Schematic diagrams of the discernible π-conjugated packing and the corresponding charge-carrier transport in a) as-spun and b) 200 °C-annealed films. (The dark regions, black lines, and arrows represent the crystalline domains, π-conjugated polymer chains, and charge transport pathways, respectively.)

negligible V_G-sweep hysteresis. Owing to the benefit of efficient π-conjugated self-assembly of the semiconducting polymer and its narrow π-overlapping distance, even the OFET fabricated from as-spun PDPP-TVT-29 delivered high electrical performance: μ_{FET} = 1.3 cm^2 V^{-1} s^{-1}, threshold voltage V_{th} = −4 V, on/off current ratio $I_{ON}/I_{OFF} > 10^6$, and subthreshold swing SS = 0.31 V decade^{-1}. As expected, short-term annealing at T_A = 200 °C enabled the OFETs tested here to exhibit the highest μ_{FET} of up to 3.7 cm^2 V^{-1} s^{-1}. In addition, OFETs that were annealed at 200 °C yielded I_D values that were three times the value obtained for the OFET based on the as-spun film, as shown in Figure 6d. However, thermal annealing at temperatures exceeding 200 °C produced deep pin-holes and less ordered π-conjugated overlap of PDPP-TVT-29 chains, thereby causing degradation of the electrical performances: μ_{FET} (3.7 cm^2 V^{-1} s^{-1}) at T_A of 200 °C was decreased to 1.8 cm^2 V^{-1} s^{-1}.

3. Conclusion

A donor–acceptor DPP-thiophene vinylene thiophene (TVT) copolymer (PDPP-TVT) with a long, linear, space-separated, branched 7-decylnonadecyl side-chain had excellent solubility in various solvents and good thermal stability. The AFM and 2D GIXD results suggested that short-term thermal annealing of a PDPP-TVT-29 film (at 200 °C for 10 min) could alter the crystalline film morphology, changing the intergranular nanocrystals with a mesoscopic structure between the rods and layer to a laterally expanded layer of crystals with a step height, which originated from edge-on oriented polymers.

The as-spun PDPP-TVT-29 film showed high field-effect mobility (μ_{FET}) of up to 1.39 cm^2 V^{-1} s^{-1} in an OFET without thermal annealing, while the film annealed at 200 °C had an enhanced μ_{FET} of up to 3.71 cm^2 V^{-1} s^{-1}. The significantly high μ_{FET} observed for the thermally annealed PDPP-TVT-29 film was mainly related to the extraordinarily layered π-conjugated crystals, owing to the strong intermolecular interactions and the spaced out side-chain arrangement that helped the polymer

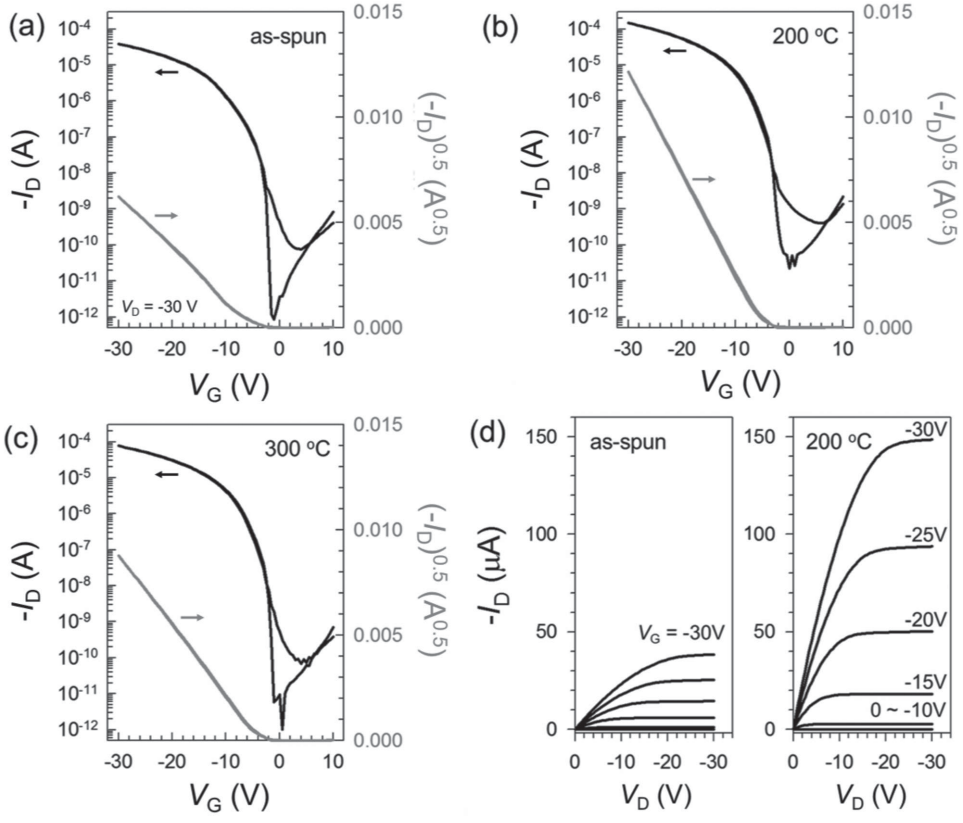

Figure 6. Typical I_D–V_G transfer curves of PDPP-TVT-29 OFETs containing a) as-spun, b) 200 °C-annealed, and c) 300 °C-annealed polymer films. d) Corresponding I_D–V_D output curves of the as-spun and 200 °C-annealed systems.

Table 2. Electrical performance of PDPP-TVT-29-based OFETs.

Device	Film treatment		μ_{FET} [$cm^2 V^{-1} s^{-1}$]		V_{th} [V]	I_{ON}/I_{OFF}	SS [V $decade^{-1}$]
			Avg.	Max.			
Pristine	As-spun		1.21 ± 0.18	1.39	−4.0	$>10^6$	0.31
200 °C-annealed		200 °C	3.23 ± 0.48	3.71	−4.5	$>10^6$	0.25
250 °C-annealed	10 min, T_A =	250 °C	2.42 ± 0.36	2.78	−5.5	$>10^6$	0.26
300 °C-annealed		300 °C	1.57 ± 0.24	1.81	−3.5	$>10^6$	0.27

chains form well-interconnected crystal grains, thus providing efficient pathways for charge transport. The highly π-conjugated nature, excellent solution processability, electrical properties, and simple synthesis of PDPP-TVT-29 suggest that the copolymer can potentially be applied to high-throughput, roll-to-roll solution printing of low-cost OFET circuits and arrays.

4. Experimental Section

Materials and Sample Preparation: The polymer PDPP-TVT-29 was synthesized via a palladium-catalyzed Stille coupling reaction, as previously described.[16] The number–average molecular weight (M_n) of PDPP-TVT-29 was 33 kDa, with a polydispersity index (PDI) of 1.8. For surface modification of the 300 nm thick, thermally grown SiO_2 on a highly n-doped Si wafer, dimethylchlorosilane-terminated polystyrene (PS-Si$(CH_3)_2$Cl, M_w = 8 kDa, PDI = 1.1; Polymer Source) was dissolved in toluene and spin-coated on the substrate in a N_2-purged glove box. The resulting films were annealed at 100 °C for 60 min, followed by rinsing with toluene and sonication in a toluene bath for 3 min to remove the unreacted residues of PS-Si$(CH_3)_2$Cl.[10] PDPP-TVT-29 was spun-cast onto the PS-grafted SiO_2 (referred to as gPS-SiO_2) dielectrics from a 2 mg mL^{-1} chloroform solution, and some of the as-spun films were thermally annealed at various values of T_A for 10 min (Figure S1, Supporting Information). The thermal evaporation of Au electrodes through a shadow mask produced the top-contact electrode of the OFET: the channel length (L) and width (W) were 100 and 1500 μm, respectively.

Characterization: The electrical characteristics of PDPP-TVT-29-based OFETs were measured at room temperature in a N_2-purged glove box using a Keithley 4200 SCS. The values of μ_{FET} and V_{th} were calculated in the saturation regime using the equation $I_D = \mu_{FET} C_i W (2L)^{-1} (V_G - V_{th})^2$, where C_i is the capacitance of the gate dielectric. The value of C_i for the dielectric, sandwiched between the Au dots and highly doped n-type Si (100) substrate, were measured using an Agilent 4284A Precision LCR meter. A synchrotron-based 2D GIXD experiment was performed on the semiconducting films at the 9A and 3C beamlines of the Pohang Light Source (PLS), Korea.

Near-Edge X-Ray Absorption of Fine Structure: All the NEXAFS measurements were performed at room temperature at the 2A and 4D beamlines of PLS. We used the PEY detection mode for the NEXAFS spectra by recording the sample current normalized to a signal current, which was measured simultaneously using a gold mesh in ultrahigh vacuum (<10^{-9} Torr). In this case, a p-polarized (≈100%) synchrotron photon beam, with an energy in the range of 279–320 eV and a spectral energy resolution of ΔE = 100 meV, had a probing depth of 6 nm for surface-sensitive measurements.

Supporting Information

Supporting Information is available from the Wiley Online Library or from the author.

Acknowledgements

This work was supported by grants from the Center for Advanced Soft Electronics under the Global Frontier Research Program (2012M3A6A5055225) and the National Research Foundation (NRF) Program (2013R1A12063963, 2012R1A2A2A06047047).

Received: October 7, 2014
Published online: May 15, 2015

[1] J. A. Rogers, Z. Bao, *J. Polym. Sci., Part A: Polym. Chem.* **2002**, *40*, 3327.
[2] G. H. Gelinck, H. E. A. Huitema, E. van Veenendaal, E. Cantatore, L. Schrijnemakers, J. B. P. H. van der Putten, T. C. T. Geuns, M. Beenhakkers, J. B. Giesbers, B.-H. Huisman, E. J. Meijer, E. M. Benito, F. J. Touwslager, A. W. Marsman, B. J. E. van Rens, D. M. de Leeuw, *Nat. Mater.* **2004**, *3*, 106.
[3] V. Subramanian, J. M. J. Frechet, P. C. Chang, D. C. Huang, J. B. Lee, S. E. Molesa, A. R. Murphy, D. R. Redinger, S. K. Volkman, *Proc. IEEE* **2005**, *93*, 1330.
[4] P. Baude, D. A. Ender, M. A. Haase, T. W. Kelley, D. V. Muyres, S. D. Theiss, *Appl. Phys. Lett.* **2003**, *82*, 3964.
[5] H. Bronstein, Z. Chen, R. S. Ashraf, W. Zhang, J. Du, J. R. Durrant, P. S. Tuladhar, K. Song, S. E. Watkins, Y. Geerts, M. M. Wienk, R. A. J. Janssen, T. Anthopoulos, H. Sirringhaus, M. Heeney, I. McCulloch, *J. Am. Chem. Soc.* **2011**, *133*, 3272.
[6] S. Qu, H. Tian, *Chem. Commun.* **2012**, *48*, 3039.
[7] T. Someya, A. Dodabalapur, J. Huang, K. C. See, H. E. Katz, *Adv. Mater.* **2010**, *22*, 3799.
[8] M. Berggren, A. Richter-Dahlfors, *Adv. Mater.* **2007**, *19*, 3012.
[9] S. Chung, M. Jang, S. B. Ji, H. Im, N. Seong, J. Ha, S. K. Kwon, Y. H. Kim, H. Yang, Y. Hong, *Adv. Mater.* **2013**, *25*, 4773.
[10] S. H. Kim, M. Jang, H. Yang, J. E. Anthony, C. E. Park, *Adv. Funct. Mater.* **2011**, *21*, 2198.
[11] H. Yang, T. J. Shin, L. Yang, K. Cho, C. Y. Ryu, Z. Bao, *Adv. Funct. Mater.* **2005**, *15*, 671.
[12] S. Qu, H. Tian, *Chem. Commun.* **2012**, *48*, 3039.
[13] H. Bronstein, Z. Chen, R. S. Ashraf, W. Zhang, J. Du, J. R. Durrant, P. S. Tuladhar, K. Song, S. E. Watkins, Y. Geerts, M. M. Wienk, R. A. J. Janssen, T. Anthopoulos, H. Sirringhaus, M. Heeney, I. McCulloch, *J. Am. Chem. Soc.* **2011**, *133*, 3272.
[14] J. C. Bijleveld, V. S. Gevaerts, D. D. Nuzzo, M. Turbiez, S. G. J. Mathijssen, D. M. de Leeuw, M. M. Wienk, R. A. J. Janssen, *Adv. Mater.* **2010**, *22*, E242.
[15] S.-Y. Liu, M.-M. Shi, J.-C. Huang, Z.-N. Jin, X.-L. Hu, J.-Y. Pan, H.-Y. Li, A. K. -Y. Jen, H.-Z. Chen, *J. Mater. Chem. A* **2013**, *1*, 2795.
[16] I. Kang, H. J. Yun, D. S. Chung, S. K. Kwon, Y. H. Kim, *J. Am. Chem. Soc.* **2013**, *135*, 14896.

[17] M. Jang, K. Y. Baek, H. Yang, *J. Phys. Chem. C* **2013**, *117*, 25290.
[18] H.-G. Jeon, J. Hattori, S. Kato, N. Oguma, N. Hirata, Y. Taniguchi, M. Ichikawa, *J. Appl. Phys.* **2010**, *108*, 124512.
[19] H. J. Chen, Y. L. Guo, G. Yu, Y. Zhao, J. Zhang, D. Gao, H. T. Liu, Y. Q. Liu, *Adv. Mater.* **2012**, *24*, 4618.
[20] R. J. Kline, M. D. McGehee, E. N. Kadnikova, J. Liu, J. M. J. Frechet, M. F. Toney, *Macromolecules* **2005**, *38*, 3312.
[21] I. McCulloch, M. Heeney, C. Bailey, K. Genevicius, I. MacDonald, M. Shkunov, D. Sparrowe, S. Tierney, R. Wagner, W. Zhang, M. L. Chabinyc, R. J. Kline, M. D. McGehee, M. F. Toney, *Nat. Mater.* **2006**, *5*, 328.
[22] L. Yang, H. Yang, *J. Synchrotron Radiat.* **2009**, *16*, 788.
[23] H.-W. Lin, W.-Y. Lee, W.-C. Chen, *J. Mater. Chem.* **2012**, *22*, 2120.
[24] Y. Li, P. Sonar, L. Murphy, W. Hong, *Energy Environ. Sci.* **2013**, *6*, 1684.
[25] J. Stöhr, *NEXAFS Spectroscopy*, 1st ed., Springer, Berlin **1996**, p. 403.
[26] D. M. DeLongchamp, R. J. Kline, D. A. Fischer, L. J. Richter, M. F. Toney, *Adv. Mater.* **2011**, *23*, 319.
[27] J. Rivnay, S. C. B. Mannsfeld, C. H. Miller, A. Salleo, M. F. Toney, *Chem. Rev.* **2012**, *112*, 5488.